Numerical evidences of a universal critical behavior of 2D and 3D random quantum clock and Potts models

Valentin Anfray, Christophe Chatelain

Numerical evidences of a universal critical behavior of 2D and 3D random quantum clock and Potts models

Valentin Anfray
Université de Lyon, Université Claude Bernard Lyon 1, CNRS, Institut Lumière Matière, F-69622 Villeurbanne, France

Christophe Chatelain
Université de Lorraine, CNRS, LPCT, F-54000 Nancy, France
(Dated: December 27, 2022)

The random quantum q-state clock and Potts models are studied in 2 and 3 dimensions. The existence of Griffiths phases is tested in the 2D case with $q = 6$ by sampling the integrated probability distribution of local susceptibilities of the equivalent McCoy-Wu 3D classical models with Monte Carlo simulations. No Griffiths phase is found for the clock model. In contrast, numerical evidences of the existence of Griffiths phases in the random Potts model are given and the Finite Size effects are analyzed. The critical point of the random quantum clock model is then studied by Strong-Disorder Renormalization Group. Despite a chaotic behavior of the Renormalization-Group flow at weak disorder, evidences are given that this critical behavior is governed by the same Infinite-Disorder Fixed Point as the Potts model, independently from the number of states q.

I. INTRODUCTION

Universality is a cornerstone of the theory of critical phenomena. At the vicinity of a continuous phase transition, the critical exponents appearing in the algebraic behavior of thermodynamic quantities are independent from the microscopic details of the system. The Renormalization Group provides a theoretical foundation to this universality[1]. The symmetry of the Hamiltonian that is spontaneously broken during the phase transition participates to determine the universality class. Universality classes may be drastically affected by the introduction of disorder in the system. The q-state Potts model, whose Hamiltonian is invariant under the permutations of the q states, is a well-known example of this principle. In two dimensions, the classical Potts model undergoes a second-order phase transition when $q \leq 4$ with critical exponents depending on the number of states q[2]. As shown by Harris, the critical behavior is unchanged in presence of randomness only if the specific heat of the pure model diverges at most logarithmically[3]. In contrast, when the specific heat exponent α is positive, randomness induces a new critical behavior. This the case for the 2D classical Potts model when $2 < q \leq 4$[4–6]. Moreover, discontinuous phase transitions are smoothed by randomness. It was proved that, in two dimensions, an infinitesimal amount of disorder is sufficient to make the transition continuous[7]. Such a situation is observed for the 2D Potts model with $q > 4$. The new critical behavior is again q-dependent[8,9].

Surprisingly, a totally different picture emerged in random quantum systems. In the models considered in the literature, the critical behavior turns out to be independent of the spontaneously-broken symmetry of the Hamiltonian. The random Ising chain in a transverse field has been extensively studied by Fisher[10–13] using a real-space Renormalization Group technique, termed as Strong-Disorder Renormalization Group (SDRG)[14]. In contrast to the pure quantum Ising chain in a transverse field, the dynamics is activated, i.e. at the critical point the gap ΔE vanishes with the lattice size L as $\Delta E \sim e^{-aL^{\psi}}$ instead of the usual law $\Delta E \sim L^{-z}$. The dynamical exponent z is therefore infinite. The exponent ψ takes the value $1/2$ because the logarithm of the renormalized couplings generated along the SDRG flow are uncorrelated random variables. The magnetic critical exponent is predicted to be equal to the golden ratio $(1+\sqrt{5})/2$. On both sides of the critical point lie two Griffiths phases where the dynamics is dominated by rare macroscopic regions with strong fluctuations of randomness. The dynamical exponent is equal to 1 at the boundary of these phases and diverges as the critical point is approached[15]. The q-state random quantum Potts chain was also studied by SDRG[16]. Note that the Ising model in a transverse field is equivalent to the $q = 2$ Potts model. The analysis of the RG flow equations showed that the number of states q is irrelevant. Therefore, the critical behavior of the random Potts chain is governed by the same Infinite Disorder Fixed Point (IDFP) as the Ising chain for any number of states q. The fact that the symmetry-group of the Hamiltonian is q-dependent does not play any role. DMRG simulations confirmed this result[17]. The q-state random quantum clock chain was also considered. In contrast to the Potts model, the Hamiltonian is invariant under circular permutations of the q states. SDRG also predicts that the critical behavior of the random clock chain is described by the same q-independent IDFP as the Ising and Potts chains at strong enough disorder[16]. This result was also confirmed by DMRG simulations[18]. Finally, the Ashkin-Teller model, corresponding to two coupled Ising chains, was studied using a numerical implementation of SDRG. Again, along the three transitions lines, the critical behavior is governed by the

same IDFP as the Ising chain. Only at the tricritical point where these lines merge, a different IDFP was identified[19–21].

An interesting question in this context is whether this super-universality is specific to one-dimensional quantum systems or also exists in higher dimensions. The random Ising model in a transverse field was studied in dimensions $d = 2, 3$ and 4 using a clever numerical implementation of SDRG[22–24]. It turns out that the critical exponents depends on the dimension d. In particular, the exponent ψ takes values smaller than 1/2, indicating that the logarithm of the renormalized couplings are now correlated. Recently, we applied the same algorithm to the 2D and 3D random Potts models and provided numerical evidences that the critical behavior is the same as the Ising model at the same dimension d for all the number of states q considered[25].

In this work, the random q-state clock and Potts models are considered. In the first section, the 3D classical analogue of the 2D random quantum 6-state clock and Potts models are studied by Monte Carlo simulations. While a phase transition is clearly seen, no Griffiths phase could be observed for the clock model. In the second section, the critical behavior of the 2D and 3D random quantum q-state clock models is determined by numerically applying the SDRG technique for several numbers of states q. It is then compared to the Potts and Ising models. Conclusions follow.

II. THE CLASSICAL 3D 6-STATE POTTS AND CLOCK MODELS

The classical q-state Potts model is defined by the Hamiltonian

$$-\beta\mathcal{H} = \sum_{(i,j)} J_{ij}\delta_{\sigma_i,\sigma_j}, \quad \sigma_i = 0, \ldots, q-1 \tag{1}$$

while for the clock model

$$-\beta\mathcal{H} = \sum_{(i,j)} J_{ij}\cos\Big(\frac{2\pi}{q}(\sigma_i - \sigma_j)\Big), \quad \sigma_i = 0, \ldots, q-1. \tag{2}$$

where $\beta = 1/k_BT$. The temperature is absorbed into the definition of the couplings. The sum extends over all pairs (i, j) of nearest-neighboring sites on the lattice. In this section, the two models are considered in the case $q = 6$ on a cubic lattice whose sizes are denoted $L_\parallel$, $L_\perp$ and $L_\perp$. In the pure case, i.e. $J_{ij} = J$, both models undergo a ferromagnetic-paramagnetic phase transition. The latter is strongly first order for the Potts model and continuous in the universality class of the 3D XY model for the clock model[26–28]. In both cases, the order parameter is the magnetization density $\frac{1}{N}|\sum_i m_i|$ where the

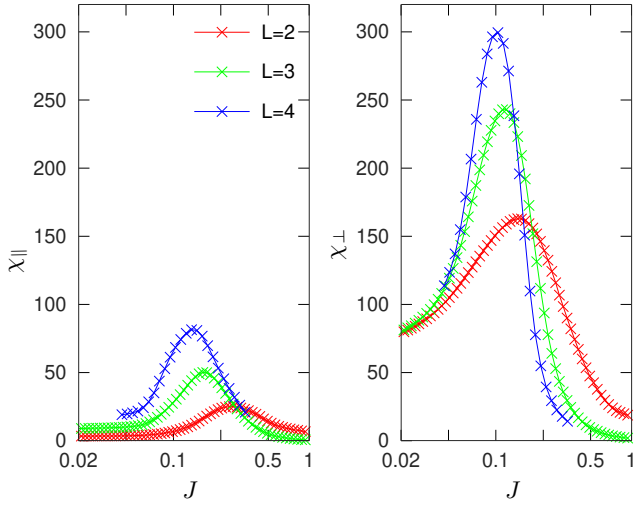

FIG. 1. Longitudinal and transverse susceptibilities $\chi_\parallel$ (left) and $\chi_\perp$ (right) of the 3D 6-state random clock model versus the weakest exchange coupling J. The different curves correspond to different transverse lattice sizes $L_\perp$. The longitudinal lattice size is $L_\parallel = 64$.

local magnetization reads

$$m_i = \frac{q\delta_{\sigma_i,0} - 1}{q - 1} \tag{3}$$

for the Potts model, and

$$m_i = e^{\frac{2i\pi}{q}\sigma_i} \tag{4}$$

for the clock model. In the following, we are interested in the random Potts and clock models with a disorder that is infinitely correlated in one direction. The couplings J_{ij} between sites i and j were chosen to depend only on the coordinates y and z of site i, i.e. they are translation-invariant in the x direction. The three couplings between site i and its neighbors on the right, at the bottom and at the back, are identical. The couplings are i.i.d random variables with the binary distribution

$$\wp(J_{ij}) = \frac{1}{2}\big(\delta(J_{ij} - J) + \delta(J_{ij} - rJ)\big). \tag{5}$$

This configuration is one of the possible generalization of the McCoy-Wu model to 3D[33]. Since the specific heat exponent of the pure 3D XY model is slightly negative[29–31], or equivalently the correlation length exponent ν is slightly larger than $2/d$, the pure fixed point of the clock model is expected to be stable upon the introduction of homogeneous disorder[3]. However, $\nu < 2/(d-1) = 1$ so the infinitely-correlated disorder that is studied in this paper is expected to be relevant. For the 6-state Potts model, the first-order phase transition of the pure model is expected to be rounded, even with an infinitesimal amount of disorder[32].

For practical reasons, we studied the clock model using the Wolff Monte Carlo algorithm[34] and the Potts model

using the Swendsen-Wang algorithm[35]. Both algorithms are equivalent in terms of convergence. In the following, one Monte Carlo Step (MCS) corresponds to $N = L_\parallel L_\perp^2$ spin flips on average. We first considered small systems, $L_\perp = 2, 3, 4$ and $L_\parallel = 64$, so that the average over all disorder configurations could be performed exactly. For $L_\perp = 4$, the number of disorder configurations is $2^{L_\perp^2} = 65536$. The reason for this choice is that we observed large deviations of the averages when computed over a smaller number of disorder configurations. The location of the phase transition can be estimated as the position of the maximum of the average magnetic susceptibility

$$\bar{\chi} = N\big[\overline{\langle m^2\rangle} - \overline{\langle m\rangle^2}\big]. \tag{6}$$

where the brackets $\langle X\rangle$ denote the average over thermal fluctuations while the above line $\overline{X}$ indicates the average over disorder. The system being strongly anisotropic, it is useful to define the two susceptibilities:

$$\begin{aligned}\bar{\chi}_\parallel &= \frac{1}{NL_\parallel}\sum_{y,z}\overline{\Big\langle\Big|\sum_x m_{(x,y,z)}\Big|^2\Big\rangle},\\ \bar{\chi}_\perp &= \frac{1}{NL_\perp^2}\sum_{x}\overline{\Big\langle\Big|\sum_{y,z} m_{(x,y,z)}\Big|^2\Big\rangle}.\end{aligned} \tag{7}$$

where $m_{(x,y,z)}$ denotes the local magnetization density on the site whose Cartesian coordinates on the cubic lattice are $(x\ y\ z)$. For both the Potts and clock models, a single peak is observed for both susceptibilities $\bar{\chi}_\parallel$ and $\bar{\chi}_\perp$, indicating the existence of a single phase transition. As can be seen on Fig. 1 for the clock model with $r = 10$, the shift of the location of the maximum of the peak is larger for $\chi_\parallel$ than for $\chi_\perp$. The same picture is qualitatively observed with a weaker disorder $r = 5$, apart from the fact that the peaks of $\chi_\parallel$ and $\chi_\perp$ are almost of same height. The truncation of the average to a small fraction of all disorder configurations leading to strong deviations, the critical behavior at the transition could be not studied by Monte Carlo simulations. In the next section, the Strong Disorder Renormalization Group will be applied to the quantum equivalent of the models. Nevertheless, the existence of Griffiths phases around the critical point can be investigated.

In a random system, large local fluctuations of the couplings allow for the existence of macroscopic ordered (resp. unordered) regions while the rest of the system is still in the paramagnetic (resp. ferromagnetic) phase[36]. The average magnetization is a non-analytic function of the magnetic field in both the ordered and disordered Griffiths phases that surrounds the critical point. As a consequence, the magnetic susceptibility diverges in the whole Griffiths phases. These singularities are too weak to be observed in classical systems with homogeneous disorder but not in the McCoy-Wu model, for which the couplings are infinitely correlated in one direction. Due to the limitation to small lattice sizes, the divergence of the susceptibility in a finite range of couplings is not observed on Fig. 1. However, the Griffiths phases also manifest themselves by an algebraic decay of the probability distribution of local linear and non-linear susceptibilities[38]. The advantage is that the method does not require an exact average over all disorder configurations. The local susceptibility is defined as

$$\chi_{\rm loc} = L_\parallel\big[\langle m_1^2\rangle - \langle m_1\rangle^2\big] \tag{8}$$

and the non-linear susceptibility (or Binder cumulant) as

$$\begin{aligned}U_{\rm loc} = L_\parallel^2\big[&\langle m_1^4\rangle - 4\langle m_1\rangle\langle m_1^3\rangle + 12\langle m_1\rangle^2\langle m_1^2\rangle\\ &-3\langle m_1^2\rangle^2 - 6\langle m_1\rangle^4\big]\end{aligned} \tag{9}$$

where the magnetization density $m_1 = \frac{1}{L_\parallel}\sum_x m_{(x,1,1)}$ is computed over the first row of the lattice only. The local susceptibility $\chi_{\rm loc}$ is related to the correlation length in the longitudinal direction:

$$\begin{aligned}\chi_{\rm loc} &= \frac{1}{L_\parallel}\sum_{x,x'}\big[\langle m_{(x,1,1)}m_{(x',1,1)}\rangle - \langle m_{(x,1,1)}\rangle^2\big]\rangle\\ &\simeq \frac{1}{L_\parallel}\int_0^{L_\parallel} e^{-|x-x'|/\xi_\parallel}dxdx'\\ &\simeq 2\xi_\parallel \qquad (\xi_\parallel \ll L_\parallel)\end{aligned} \tag{10}$$

The disordered Griffiths phase is due to clusters of strong couplings rJ that will order before the rest of the system. The probability of such a cluster of characteristic size ℓ decays exponentially fast as

$$\wp(\ell^{d_\perp}) \sim p^{\ell^{d_\perp}} \tag{11}$$

where p is the probability of a strong coupling (chosen to be $p = 1/2$ in this work) and $d_\perp = d - 1$. When the temperature T is between the critical temperature of the strong and weak couplings, this cluster tends to order ferromagnetically because the free energy gain in volume compensates the loss at its boundaries with the paramagnetic phase:

$$\Delta F = -\ell^{d_\perp}L_\parallel\big[f_{\rm o} - f_{\rm d}\big] + \ell^{d_\perp-1}L_\parallel\sigma_{\rm o,d} > 0 \tag{12}$$

where $f_{\rm o}(rJ)$ and $f_{\rm d}(J)$ are the free energy densities of the ordered and disordered homogeneous phases for strong and weak couplings respectively. $\sigma_{o,d}(J, rJ)$ is the surface tension between ordered and disordered phases. It follows from Eq. 12 that there exists a minimal size $\ell_{\rm min} = \sigma_{o,d}/[f_{\rm o} - f_{\rm d}]$ for a ferromagnetic cluster to be stable. Moreover, the long-range ordering of the cluster in the longitudinal direction may be reduced by the coexistence of different ferromagnetic phases separated by domain walls whose free energy cost is

$$\Delta F_{\rm DW} = \sigma_{o,o}\ell^{d_\perp} \tag{13}$$

per domain wall, where $\sigma_{o,o}$ is the surface tension between two ordered phases. The average size of a magnetic domain is therefore related to the size of the cluster as

$$\xi_\parallel \sim e^{\beta\sigma_{o,o}\ell^{d_\perp}} \tag{14}$$

Since $\xi_\parallel \simeq \chi_{\rm loc}$ according to Eq. 10, and since the probability of a cluster of strong couplings of characteristic size ℓ decays algebraically with $\ell_\perp^d$ as Eq. 11, it follows that $\wp(\ln \chi_{\rm loc}) \simeq \wp(\ln \xi_\parallel) \sim \wp(\ell^d)$ and therefore[38]

$$\ln \wp(\ln \chi_{\rm loc}) = {\rm Cst} - \frac{d_\perp}{z} \ln \chi_{\rm loc} \qquad (15)$$

where $d_\perp/z = -\ln p \frac{k_B T}{\sigma_{o,o}}$. The same behavior is expected for the Binder cumulant but with a coefficient $d_\perp/3z$ instead of $d_\perp/z$. This prediction has been exploited to estimate the dynamical exponent z of the transverse-field Ising spin-glass[37,38] and of the random Ising ferromagnet[39]. Note finally that the average susceptibility $\overline{\chi_{\rm loc}} = \int \chi_{\rm loc} \wp(\chi_{\rm loc}) d\chi_{\rm loc}$ diverges when $z > 1/d_\perp$.

We performed Monte Carlo simulations of the random clock and Potts models with lattice sizes $L_\perp = 12$ and $L_\parallel = 128, 256, 1024$ and 4096. The system was thermalized with 1000 MC iterations and thermal averages were then computed over 10000 MC iterations. 10000 random configurations were sampled for $L_\parallel \leq 1024$ and 1000 for $L_\parallel = 4096$. We computed the integrated probability distributions $1 - F(\chi_{\rm loc})$ and $F(U_{\rm loc})$ that are expected to display the same algebraic decay in Griffiths phases as $\wp(\ln \chi_{\rm loc})$ and $\wp(\ln U_{\rm loc})$. Examples of integrated probability distributions of both $\chi_{\rm loc}$ and $U_{\rm loc}$ are plotted in figures 2 to 3. For the clock model, we could not find any coupling J for which the integrated probability distributions of both $\chi_{\rm loc}$ and $U_{\rm loc}$ display a clear algebraic decay. The only coupling for which $1 - F(\chi_{\rm loc})$ can reasonably be fitted with a power-law over a small range of susceptibilities $\chi_{\rm loc}$ is shown on Fig. 2. The fit is plotted as a dashed line which was slightly shifted vertically to be visible. The associated dynamical exponent is $z \simeq 3.8$ at large lattice size $L_\parallel$. However, the integrated probability distribution $F(U_{\rm loc})$ does not display any algebraic decay at the same coupling. Our conclusion is that there is no Griffiths phase in the phase diagram of the random clock model.

The situation is different for the Potts model. At $J = 0.1156$ (Fig. 3), both the integrated probability distributions $1 - F(\chi_{\rm loc})$ and $F(U_{\rm loc})$ display an algebraic decay over several decades. The slopes of the curves in a log-log scale give estimates of the dynamical exponent around $z \simeq 0.8$. The latter being larger than $1/d_\perp = 1/2$, the system is in a Griffiths phase. At smaller couplings, closer to the critical point, the dynamical exponent is expected to be larger. However, an algebraic decay is still observed on Fig. 4 ($J = 0.1037$) and 5 ($J = 0.0951$) but over a smaller range of susceptibilities. Various Finite-Size effects can be invoked to explain the shape of the curves. A first regime, where the decay is slow and not algebraic, is observed at small susceptibilities $\chi_{\rm loc}$ and $U_{\rm loc}$. This regime is due to clusters that are too small to satisfy Eq. 12, i.e. $\ell < \ell_{\rm min}$. At intermediate susceptibilities, an algebraic decay is observed but with a

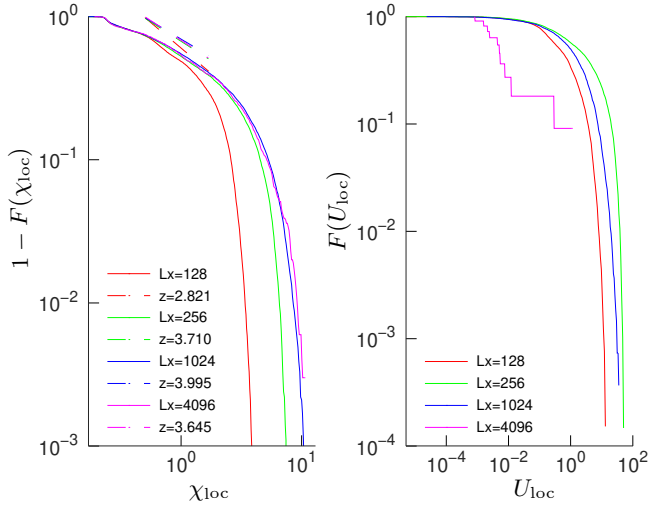

FIG. 2. Integrated probability distribution of the local susceptibility $\chi_{\rm loc}$ (left) and of the Binder cumulant $U_{\rm loc}$ (right) of the 6-state random clock model at $J = 0.0772$ and $r = 10$. The different curves correspond to different longitudinal lattice sizes $L_\parallel$. The transverse lattice size is $L_\perp = 12$.

strong dependence on the longitudinal lattice size $L_\parallel$. This dependence can be attributed to Eq. 10. For large correlation lengths $\xi_\parallel$, one should replace Eq. 10 by (with Periodic Boundary Conditions)

$$\chi_{\rm loc} \simeq 2\xi_\parallel \left(1 - e^{-L_\parallel/\xi_\parallel}\right) \qquad (16)$$

which leads to a probability distribution $\wp(\ln \chi_{\rm loc}) = \wp(\ln \xi_\parallel) \frac{d \ln \xi_\parallel}{d \ln \chi_{\rm loc}}$ that depends on $L_\parallel$, in contrast to Eq. 15. Finally, at large susceptibilities, the probability distributions fall down much faster than a power-law. This is due to the fact that the size ℓ of the clusters is bounded by the transverse lattice size $L_\perp$. As a consequence, the susceptibility $\chi_{\rm loc}$ cannot be larger than $e^{\beta \sigma_{o,o} L_\perp^{d_\perp}}$. In conclusion, we infer that the random Potts model is in a Griffiths phase for $J = 0.0951$ and 0.1037 but that Finite-Size effects are strong and explain why the algebraic decay is observed only over a smaller range of susceptibilities. The dynamical exponents that can be estimated using Eq. 15 are, as expected, large. However, they strongly depends on $L_\parallel$. These estimates should be considered with caution because a more accurate estimate would require to use the exact $L_\parallel$-dependent expression of $\wp(\ln \chi_{\rm loc})$ and not Eq. 15 that is valid only in the limit $\xi_\parallel \ll L_\parallel$.

III. CRITICAL BEHAVIOR OF 2D AND 3D RANDOM QUANTUM CLOCK MODELS

In this section, the critical behavior of the 2D and 3D random quantum q-state clock model is studied by Strong Disorder Renormalization Group. Note that the 2D and 3D random quantum q-state Potts models have been considered in Ref.[25]. In the extreme anisotropic

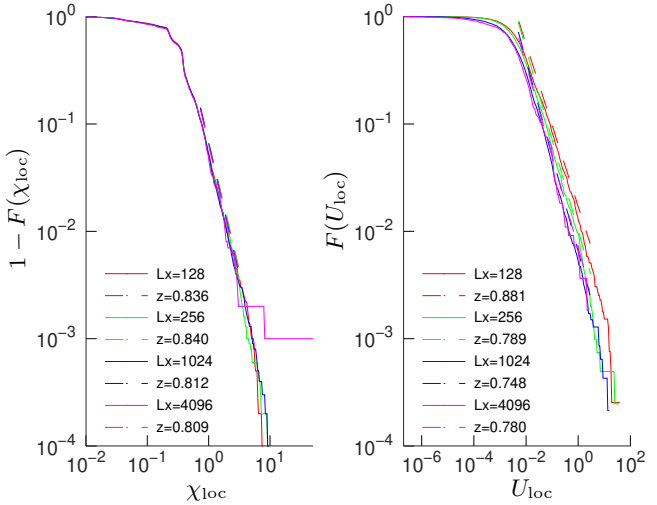

FIG. 3. Integrated probability distribution of the local susceptibility $\chi_{\rm loc}$ (left) and of the Binder cumulant $U_{\rm loc}$ (right) of the 6-state random Potts model at $J = 0.1156$ and $r = 10$. The different curves correspond to different longitudinal lattice sizes $L_\parallel$. The transverse lattice size is $L_\perp = 12$.

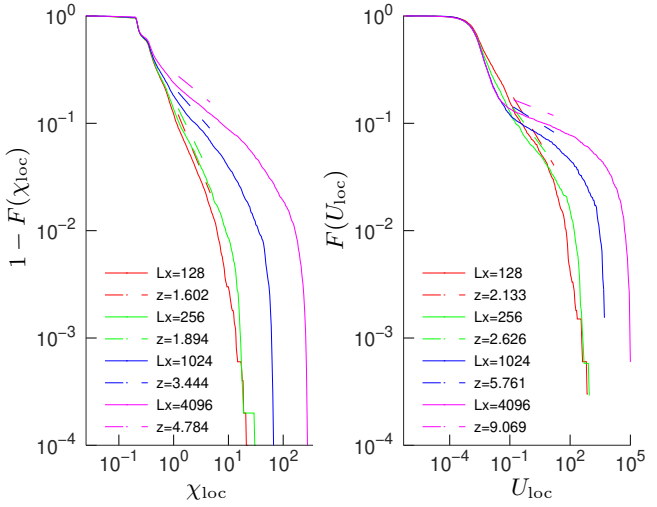

FIG. 4. Integrated probability distribution of the local susceptibility $\chi_{\rm loc}$ (left) and of the Binder cumulant $U_{\rm loc}$ (right) of the 6-state random Potts model at $J = 0.1037$ and $r = 10$. The different curves correspond to different longitudinal lattice sizes $L_\parallel$. The transverse lattice size is $L_\perp = 12$.

limit, the transfer matrix of the classical q-state clock model (Eq. 2) in dimension $d+1$ is equivalent to the imaginary-time evolution operator of the quantum clock model in dimension d whose Hamiltonian is

$$H = -\sum_{(i,j)} J_{ij}\left(\Omega_i\Omega_j^+ + \Omega_j\Omega_i^+\right) - \sum_i h_i\left(M_i + M_i^+\right) \quad (17)$$

where the sum extends over nearest neighbors on the lattice. The operator Ω_i acts only on the spin on site i, i.e. $\Omega_i = 1^{\otimes i-1} \otimes \Omega \otimes 1^{\otimes N-i}$ where N is the number of sites of the lattice. The matrix Ω is a $q \times q$ diagonal

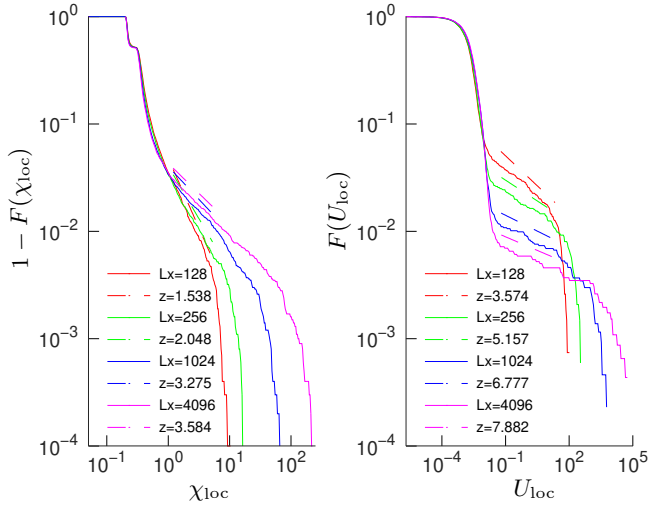

FIG. 5. Integrated probability distribution of the local susceptibility $\chi_{\rm loc}$ (left) and of the Binder cumulant $U_{\rm loc}$ (right) of the 6-state random Potts model at $J = 0.0951$ and $r = 10$. The different curves correspond to different longitudinal lattice sizes $L_\parallel$. The transverse lattice size is $L_\perp = 12$.

matrix whose elements are ω^n with $\omega = e^{2i\pi/q}$. Similarly, $M_i = 1^{\otimes i-1} \otimes M \otimes 1^{\otimes N-i}$ and M is the $q \times q$ matrix whose only non-zero elements are equal to 1 and are on the diagonal above the main diagonal. The couplings J_{ij} and h_i are positive, random and uncorrelated.

A. SDRG decimation rules and chaoticity of the RG flow

The SDRG decimation rules are easily derived for the q-state clock model[16]. When the largest coupling is $\Omega = J_{ij}$, the Hamiltonian (17) is projected onto the ground state of the local Hamiltonian $-J_{ij}\left(\Omega_i\Omega_j^+ + \Omega_j\Omega_i^+\right)$. Since the latter is q-fold degenerated, the two spins on sites i and j are replaced by an effective q-state macro-spin. Second-order perturbation theory shows that this macro-spin is coupled to an effective transverse field

$$\tilde{h} = \frac{h_i h_j}{\kappa J_{ij}} \quad (18)$$

where $\kappa = 1 - \cos 2\pi/q$ for $q > 2$ and to all the neighbors of sites i and j by a coupling $J_{ik} + J_{jk}$. When the largest coupling is $\Omega = h_i$, the spin is frozen in the ground state of the local Hamiltonian $-h_i\left(M_i + M_i^+\right)$. An effective coupling between any pairs (k,l) of neighboring sites coupled to i is induced at second-order perturbation theory:

$$\tilde{J}_{kl} = J_{kl} + \frac{J_{ki}J_{il}}{\kappa h_i}. \quad (19)$$

For the q-state Potts model, the same decimation rules are obtained but with $\kappa = q/2$. This small difference has however important consequences. For the Potts model,

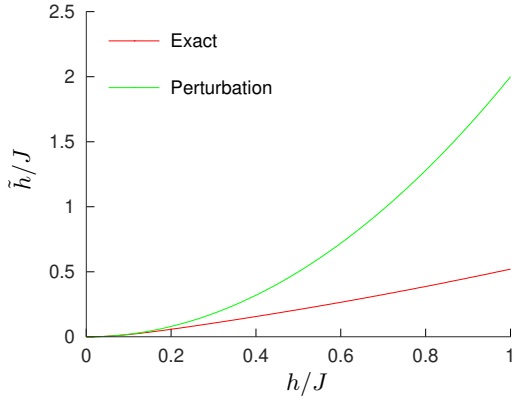

FIG. 6. Effective transverse field $\tilde{h}$ versus h/J ($h_1 = h_2 = h$) computed either by second-order perturbation theory (18) or by exact diagonalization of the two-site Hamiltonian $-J(\Omega_1\Omega_2^+ + \Omega_2\Omega_1)^+ - h(M_1 + M_1^+) - h(M_2 + M_2^+)$ for the 6-state clock model. In the second case, the effective transverse field is extracted from the gap ΔE between the first excited state and the ground state as $\tilde{h} = \Delta E/2\kappa$.

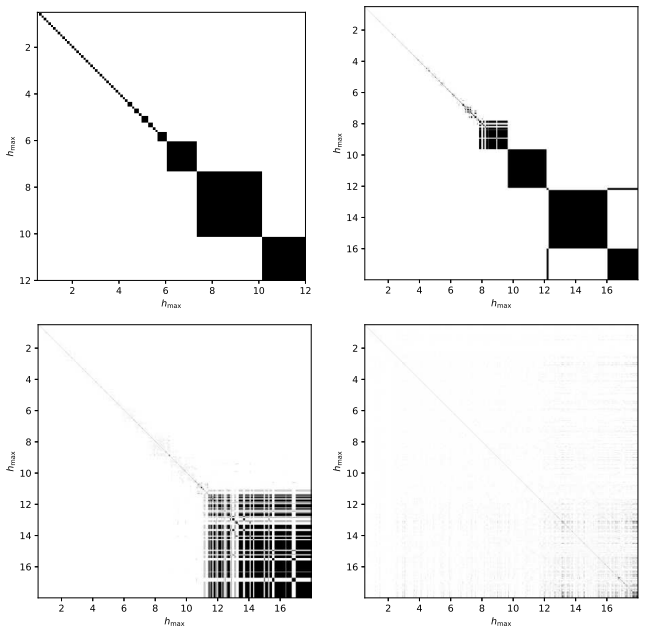

FIG. 7. Recurrence matrices for a 32×32 clock model with uniform distributions $P_0(J_{ij})$ and $Q_0(h_i)$ of the initial couplings. The number of states of the clock model is 2 (top left), 6 (top right), 8 (bottom left) and 10 (bottom right).

the effective coupling is always smaller than Ω. It is not always the case for the clock model since $\kappa < 1$ for $q > 4$. When a bond $\Omega = J_{ij}$ is decimated, an effective transverse field $\tilde{h}$ larger than Ω can be generated when the two transverse fields h_i and h_j are large, more precisely when $h_i h_j > \kappa\Omega$ although $h_i, h_j < \Omega$. This large induced transverse field $\tilde{h}$ is not physical and comes from the fact that the renormalized couplings are computed using second-order perturbation theory. At higher orders, the renormalized couplings are expected to remain smaller than Ω. As can be seen on Fig. 6, the comparison with an exact diagonalization of the 2-site Hamiltonian shows that the use of second-order perturbation theory is justified when $h_1, h_2 \lesssim 0.2 J_{ij}$ for the 6-state clock model while the effective transverse field becomes larger than $\Omega = J_{ij}$ when $h_1, h_2 \simeq 0.7 J_{ij}$. The consequences of this are severe only far from the IDFP. As the IDFP is approached, the probability distribution of the couplings becomes broader and broader. As a consequence, the probability that $h_i h_j > \kappa\Omega$, and therefore that an effective transverse field $\tilde{h} > \Omega$ be induced by the decimation of J_{ij}, becomes smaller and smaller. However, numerical simulations are limited to finite systems and therefore to a finite number of RG steps. For small systems, the simulation may end up still relatively far from the IDFP. We observed that renormalized couplings $\tilde{h}, \tilde{J} > \Omega$ slow down the convergence of the RG flow towards the IDFP. In some situations, the RG flow can even become chaotic. Note that the renormalized couplings are proportional to $1/\kappa$ so the effect is stronger for clock models with large numbers of states q.

One way to overcome the problem posed by large renormalized couplings is to modify the decimation rules, either by including higher-orders in perturbation or simply by using *ad-hoc* effective couplings equal to (18) and (19) in the limit $\tilde{h}, \tilde{J} \ll \Omega$. Another possibility is to start the simulation with broad initial distributions of the couplings h_i, J_{ij}, close to those expected at the IDFP. We used a SDRG algorithm similar to the one employed for the Potts model[25] but with a decimation of the global maximum and not of the local maximum. This algorithm has the advantage to limit drastically the number of new lattice bonds generated during the RG flow by the use of maximum rule but it requires the effective couplings to be of the form (18) and (19). As a consequence, we will avoid large effective couplings by starting the simulations with broad coupling distributions

$$P_0(J_{ij}) \sim J_{ij}^{1/\Delta - 1}, \quad (0 < J_{ij} < 1)$$
$$Q_0(h_i) \sim h_i^{1/\Delta - 1}, \quad (0 < h_i < h_{\max}). \qquad (20)$$

where Δ is a free parameter controlling the broadness of the distributions and therefore the strength of the distribution. $\theta = \ln h_{\max}$ plays the role of the control parameter of the quantum phase transition. At large (resp. small) $\ln h_{\max}$, the system is expected to be in the paramagnetic phase (resp. ferromagnetic phase).

The chaotic nature of the RG flow manifests itself in the behavior of the average magnetic moment $\bar{\mu}$ of the last cluster at the end of the RG procedure. The latter is expected to be a smooth function of $h_{\max}$. However, we observed that it is not the case for weak initial disorder or large number of states q. To demonstrate the appearance of chaoticity, we applied the RG procedure to the same disorder realization for n values $h_1 < h_2 < \ldots < h_n$ of the maximal transverse field $h_{\max}$ and measured the

magnetic moment $\mu_i = \mu(h_i)$ of the last macro-spin. A $n \times n$ recurrence matrix R is constructed as $R_{ij} = 1$ if $\mu_i = \mu_j$ and $R_{ij} = 0$ otherwise. The matrix is plotted on Fig. 7 for four different numbers of states q of the clock model. For $q = 2$, the matrix is block diagonal: the magnetic moment is a monotonous non-chaotic step function of the control parameter $h_{\max}$. In contrast, for $q = 10$, the magnetic moment oscillates widely with $h_{\max}$ and, as a consequence, the recurrence matrix becomes noisy. Fig. 7 shows that chaoticity increases with the number of states q. We have also considered the recurrence matrices for a fixed number of states q and an increasing strength of disorder Δ. As mentioned earlier, chaoticity decreases with Δ. In the next section, Δ is always chosen sufficiently large to avoid, or at least strongly suppress, the chaoticity of the RG flow.

B. Critical exponents at the IDFP

We considered quantum q-state clock models with $q = 5, 8$ and 10. We added the cases $q = 2$ and 3 that are equivalent to the Potts models and were already studied[25]. Lattice sizes up to $L = 768$ (1536 in some cases) have been reached in 2D and $L = 90$ (120 in some cases) in 3D. Averages were performed over at least 8.10^3 disorder realizations. In the following, we will use the control parameter $\theta = \ln h_{\max}$.

The control parameter $\theta_c(L)$ at the critical point is estimated using the doubling method for each random sample[22,23]. The SDRG procedure is applied to two replicas of the same system with the same disorder configuration coupled together at their boundaries. The pseudo-critical point $\theta_c(L)$ is localized iteratively by using the fact that the magnetic moment of the last cluster of the replicated system is expected to be twice the magnetization of a single replica in the ferromagnetic phase but the same in the paramagnetic phase. For large lattice sizes L, the average pseudo-critical control parameter $\overline{\theta_c(L)}$ displays the power-law behavior

$$|\overline{\theta_c(L)} - \theta_c| \sim L^{-1/\nu}. \tag{21}$$

The data are shown on Fig 8 in the case of the 2D and 3D random 10-state clock model. The critical exponent ν has been estimated by a non-linear fit with the law Eq. 21. However, although small, the existence of scaling corrections can be seen on the data, especially in 3D. To take them into account, we restricted the fit to lattice sizes $L > L_{\min}$ and repeated the operation with increasing sizes $L_{\min}$. The effective exponents $\nu(L_{\min})$ given by these fits are plotted versus $1/L_{\min}$ in Fig .9. Most of the points are compatible within error bars and no indication of a dependence on the number of states q is observed. Extrapolating to $L_{\min} \to +\infty$, the exponent can be estimated to be $\nu \simeq 1.24(3)$ in 2D and 0.99(3) in 3D. These values are in agreement with those obtained for the Potts model: $\nu \simeq 1.25(6)$ in the 2D case and 1.01(5) in 3D[25].

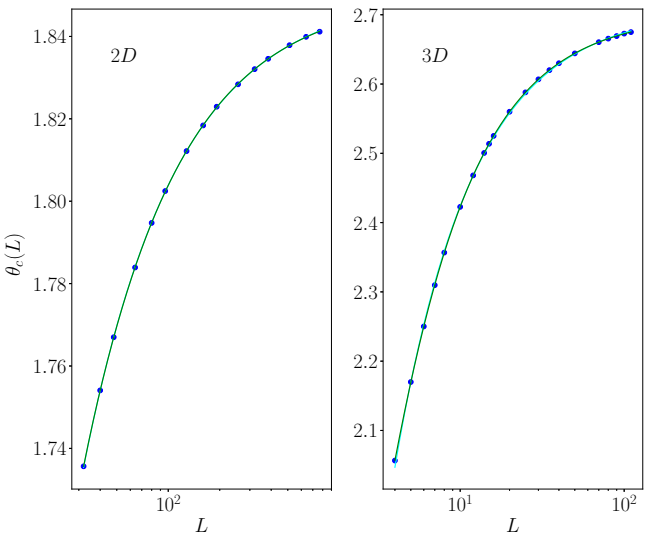

FIG. 8. Average control parameter $\overline{\theta_c(L)}$ at the pseudo-critical critical point versus the lattice L for the 2D (left) and 3D (right) random 10-state clock model with $\Delta = 5$. The blue curve corresponds to a fit to Eq. (21) while scaling corrections are taken into account in the fit plotted in green color. As can be seen, the two curves can hardly be distinguished.

The strong dependence of the effective exponent on $L_{\min}$ in 3D suggests the existence of q-dependent scaling corrections. We have also performed fits with the scaling law $|\overline{\theta_c(L)} - \theta_c| \sim L^{-1/\nu}(1 + aL^{-\omega})$ including the first scaling correction. However, the fit becomes unstable and the error bars on ν are large in the 2D case while it gives compatibles estimates of ν for 3D clock models.

The critical exponent ν can also be estimated from the Finite-Size Scaling of the standard deviation of the pseudo-critical points $\Delta\theta_c(L) = [\overline{(\theta_c(L))^2} - \overline{\theta_c(L)}^2]^{1/2}$. The same procedure as above is applied to take into account scaling corrections. The effective exponents $\nu(L_{\min})$ are presented on Fig. 10 in the case of the 10-state random clock model. In the limit $L_{\min} \to +\infty$, the critical exponents are estimated to be $\nu \simeq 1.24(2)$ in the 2D case and 0.99(1) in 3D. These values are in agreement with those obtained for the Potts model: $\nu \simeq 1.25(3)$ in the 2D case and 0.985(10) in 3D[25].

The average magnetic moment of the last macro-spin at the end of the RG process is expected to scale as

$$\bar{\mu} \sim L^{d_f} \tag{22}$$

Effective fractal dimensions $d_f(L_{\min})$ are computed by a simple power-law fit. The estimates are presented on Fig. 11 versus the smallest lattice size $L_{\min}$ considered in the fit. In the 2D case, the effective exponents for different numbers of states q get closer when $L_{\min}$ is increased but they are still incompatible in the limit $L_{\min} \to +\infty$ when considering the error bars. We note however that, when the disorder strength Δ is increased, the effective

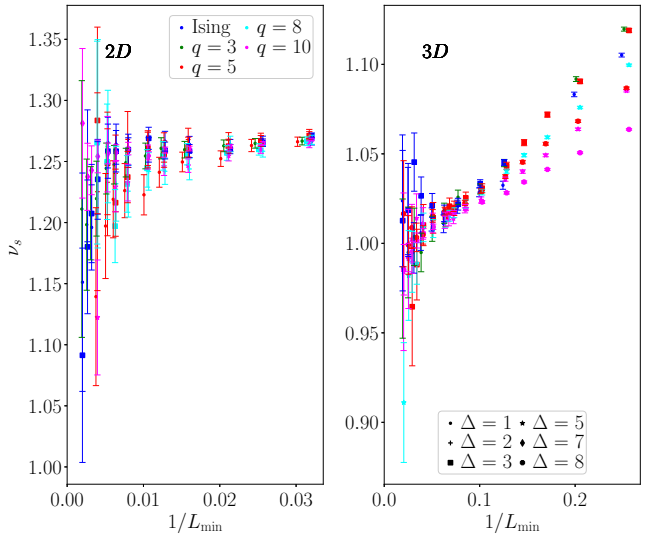

FIG. 9. Critical exponent ν extracted from the finite-size behavior of the shift of the average control parameter $\overline{\theta_c(L)}$ at the pseudo-critical critical point versus the inverse $1/L_{\min}$ of the smallest lattice size $L_{\min}$ taken into account in the fit. The left figure corresponds to the 2D random q-state clock model and the right one to the 3D model. The color of the symbols is related to the number of states q and their shape to the strength of the initial disorder.

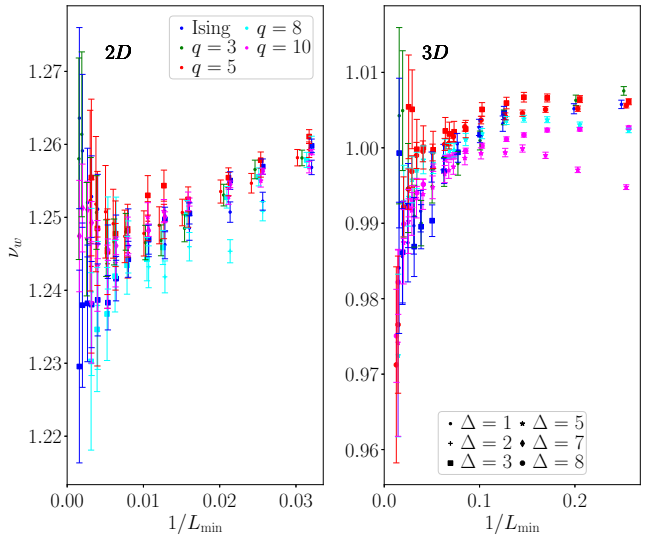

FIG. 10. Critical exponent ν extracted from the finite-size behavior of the standard deviation $\Delta\theta_c(L)$ of the control parameter at the pseudo-critical critical point versus the inverse $1/L_{\min}$ of the smallest lattice size $L_{\min}$ taken into account in the fit. The left figure corresponds to the 2D random q-state clock model and the right one to the 3D model. The color of the symbols is related to the number of states q and their shape to the strength of the initial disorder.

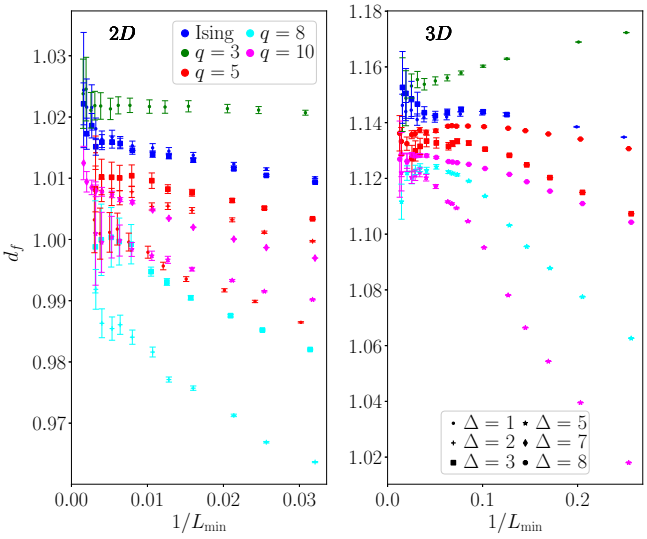

FIG. 11. Magnetic fractal dimension d_f extracted from the finite-size behavior of the average magnetic moment $\bar{\mu}$ of the last cluster versus the inverse $1/L_{\min}$ of the smallest lattice size $L_{\min}$ taken into account in the fit. The left figure corresponds to the 2D random q-state clock model and the right one to the 3D model. The color of the symbols is related to the number of states q and their shape to the strength of the initial disorder.

fractal dimensions $d_f(L_{\min})$ of the Ising model ($q = 2$) are relatively stable. The effective fractal dimensions for $q = 8, 10$ and 5 are systematically lower than the Ising values but the difference is much smaller at strong disorder than at weak disorder. It is therefore plausible that the fractal dimensions eventually become compatible for all q-state clock models at stronger disorders. The Ising estimates being the more stable, the fractal dimension would be $d_f \simeq 1.018$. Note that it was shown that the fractal dimensions of the 2D q-state random Potts model is compatible with this value (1.021(5)) for all number of states q[25]. A strong dependence of the scaling corrections on the disorder strength Δ is also observed in the 3D case. The effect is particularly important for the $q = 10$ clock model: the slope of the effective fractal dimensions $d_f(L_{\min})$ depends strongly on the disorder strength. Nevertheless, for the strongest disorder $\Delta = 8$, the fractal dimensions of the $q = 5$ and 10-clock models are compatible within errors bars with the value $d_f \simeq 1.132(6)$. The latter is close, although not compatible within error bars, with the estimate 1.155(8) of the fractal dimension of the 3D random q-state Potts model[25].

The dynamical exponent being infinite at the IDFP, the energy gap scales with the lattice size as

$$\Delta E \sim a\, e^{-b\, L^{\psi}} \tag{23}$$

where a and b are two constants. An effective exponent $\psi(L_{\min})$ is estimated by a non-linear fit of the average $\overline{\ln \Delta E}$ of the logarithm of the energy gap as $\ln a + b\, L^{\psi}$. The estimates of this exponent are presented on Fig. 12.

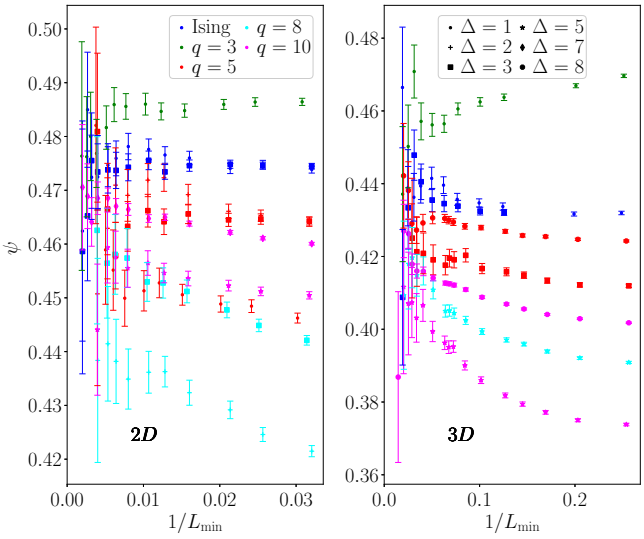

FIG. 12. Critical exponent ψ extracted from the finite-size behavior of the logarithm of the energy gap $\overline{\ln \Delta E}$ of the last cluster versus the inverse $1/L_{\min}$ of the smallest lattice size $L_{\min}$ taken into account in the fit. The left figure corresponds to the 2D random q-state clock model and the right one to the 3D model. The color of the symbols is related to the number of states q and their shape to the strength of the initial disorder.

The error bars are much larger than for the fractal dimensions d_f and the exponents ν. Again, the scaling corrections are observed to depend both on the number of states q and on the disorder strength Δ. In the 2D case, when considering only the disorder strengths $\Delta \geq 3$, the effective critical exponents in the limit $L_{\min} \to +\infty$ are compatible within error bars with the value $\psi \simeq 0.467(10)$. They are also compatible with the estimate 0.48(2) obtained for the 2D random quantum Potts model[25]. In the 3D case, the error bars are even larger. For disorder strength $\Delta \geq 3$, the critical exponents are compatible with $\psi \simeq 0.43(2)$. For the strongest disorder considered $\Delta = 8$, the $q = 5$ and 10 clock models are compatible with the value $\psi \simeq 0.425(5)$. For the 3D random quantum Potts model, the estimate was 0.46(4)[25].

ACKNOWLEDGMENTS

The numerical simulations of this work were performed at the meso-center eXplor of the université de Lorraine under the project 2018M4XXX0118.

IV. CONCLUSIONS

We have analyzed the phase transition undergone by the 2D and 3D random quantum clock and Potts models. By studying the analogue of the classical McCoy-Wu model, a single phase transition is observed as a peak of the magnetic susceptibility. It is however not possible with our data to decide whether the susceptibility diverges only at one critical temperature or over a finite range of temperatures as expected in Griffiths phases. The lattice sizes for which an exact average over disorder can be performed are too small. We then analyzed the integrated probability distribution of the logarithm of the local susceptibilities which is expected to decay algebraically in Griffiths phases[38]. No such decay could be observed for the clock model. In contrast, an algebraic decay is clearly observed over a wide range of several decades for the Potts model. However, close to the critical point, this range is reduced by strong Finite-Size effects. These effects could be interpreted in light of the physical mechanism proposed in Ref.[38]. Nevertheless, it is not clear to us why the Potts model display Griffiths phase whereas the clock model does not. A possible explanation of the absence of Griffiths phase could be that $\ell_{\min} > L_\perp$ for the clock model, i.e. a simple Finite-Size effect. It is also possible that Griffiths phases would appear at stronger disorder.

In the second section of this paper, we studied the critical behavior of the 2D and 3D random quantum clock models by Strong Disorder Renormalization Group (SDRG) and compared the estimated exponents with the known values for the Ising and Potts models. We have shown that the use of second-order perturbation theory in the determination of the SDRG rules are responsible for a chaotic behavior of the RG flow at weak disorder. Nevertheless, at strong enough disorder, our estimates of the critical exponents are compatible, or at least close in some cases, to the Ising and Potts values leading to the conclusion that the super-universality class of the random Ising and Potts models encompasses the clock model for any number of states.

V. BIBLIOGRAPHY

[1] J. Cardy, *Scaling and Renormalization in Statistical Physics*, Cambridge University Press (1996).

[2] F. Y. Wu, *The Potts Model*, Rev. Mod. Phys. **54**, 235

(1982).
[3] A. B. Harris, *Effect of Random Defects on the Critical Behaviour of Ising Models*, J. Phys. C: Solid State Physics **7**, 1671 (1974).
[4] A. W. W. Ludwig, *Critical Behavior of the Two-Dimensional Random q-State Potts Model by Expansion in* $(q-2)$, Nucl. Phys. B **285**, 97 (1987).
[5] V. Dotsenko, M. Picco, and P. Pujol, *Renormalisation-Group Calculation of Correlation Functions for the 2D Random Bond Ising and Potts Models*, Nucl. Phys. B **455**, 701 (1995).
[6] C. Chatelain and B. Berche, *Universality and Multifractal Behaviour of Spin-Spin Correlation Functions in Disordered Potts Models*, Nuclear Physics B **572**, 626 (2000).
[7] M. Aizenman and J. Wehr, *Rounding of First-Order Phase Transitions in Systems with Quenched Disorder*, Phys. Rev. Lett. **62**, 2503 (1989).
[8] J. Cardy and J. L. Jacobsen, *Critical Behavior of Random-Bond Potts Models*, Phys. Rev. Lett. **79**, 4063 (1997).
[9] C. Chatelain and B. Berche, *Magnetic Critical Behavior of Two-Dimensional Random-Bond Potts Ferromagnets in Confined Geometries*, Phys. Rev. E **60**, 3853 (1999).
[10] D. S. Fisher, *Random Transverse Field Ising Spin Chains*, Phys. Rev. Lett. **69**, 534 (1992).
[11] D. S. Fisher, *Critical Behavior of Random Transverse-Field Ising Spin Chains*, Phys. Rev. B **51**, 6411 (1995).
[12] F. Iglói and C. Monthus, *Strong Disorder RG Approach of Random Systems*, Physics Reports **412**, 277 (2005).
[13] F. Iglói and C. Monthus, *Strong disorder RG approach – a short review of recent developments*, Eur. Phys. J. B **91**, 290 (2018).
[14] C. Dasgupta and S. Ma, *Low-Temperature Properties of the Random Heisenberg Antiferromagnetic Chain*, Phys. Rev. B **22**, 1305 (1980).
[15] F. Iglói, *Exact Renormalization of the Random Transverse-Field Ising Spin Chain in the Strongly Ordered and Strongly Disordered Griffiths Phases*, Phys. Rev. B **65**, 064416 (2002).
[16] T. Senthil and S. N. Majumdar, *Critical Properties of Random Quantum Potts and Clock Models*, Phys. Rev. Lett. **76**, 3001 (1996).
[17] E. Carlon, C. Chatelain, and B. Berche, *Critical Behavior of the Random Potts Chain*, Phys. Rev. B **60**, 12974 (1999).
[18] E. Carlon, P. Lajkó, and F. Iglói, *Disorder Induced Cross-Over Effects at Quantum Critical Points*, Phys. Rev. Lett. **87**, 277201 (2001).
[19] F. Hrahsheh, J. A. Hoyos, R. Narayanan, and T. Vojta, *Strong-Randomness Infinite-Coupling Phase in a Random Quantum Spin Chain*, Phys. Rev. B **89**, 014401 (2014).
[20] H. Barghathi, F. Hrahsheh, J. A. Hoyos, R. Narayanan, and T. Vojta, *Strong-Randomness Phenomena in Quantum Ashkin–Teller Models*, Phys. Scr. T **165**, 014040 (2015).
[21] C. Chatelain and D. Voliotis, *Numerical Evidence of the Double-Griffiths Phase of the Random Quantum Ashkin-Teller Chain*, Eur. Phys. J. B **89**, 18 (2016).
[22] I. A. Kovács and F. Iglói, *Renormalization Group Study of the Two-Dimensional Random Transverse-Field Ising Model*, Phys. Rev. B **82**, 054437 (2010).
[23] I. A. Kovács and F. Iglói, *Infinite-Disorder Scaling of Random Quantum Magnets in Three and Higher Dimensions*, Phys. Rev. B **83**, 174207 (2011).
[24] I. A. Kovács and F. Iglói, *Renormalization group study of random quantum magnets*, J. Phys.: Condens. Matter **23** 404204 (2011).
[25] V. Anfray and C. Chatelain, *Numerical Evidence of Superuniversality of the Two-Dimensional and Three-Dimensional Random Quantum Potts Models*, Phys. Rev. B **103**, 174207 (2021).
[26] P. D. Scholten and D. R. King, *Monte Carlo Study of the Three-Dimensional Chiral Clock Model*, Phys. Rev. B **53**, 3359 (1996).
[27] S. Miyashita, *Nature of the Ordered Phase and the Critical Properties of the Three Dimensional Six-State Clock Model*, J. Phys. Soc. Jpn. **66**, 3411 (1997).
[28] J. Hove and A. Sudbø, *Criticality versus q in the* $(2+1)$*-Dimensional* Z_q *Clock Model*, Phys. Rev. E **68**, 046107 (2003).
[29] A. P. Gottlob, M. Hasenbusch, and S. Meyer, *Critical Behaviourof the 3D XY-Model: A Monte Carlo Study*, Nucl. Phys. B - Proc. Supp. **30**, 838 (1993).
[30] M. Campostrini, M. Hasenbusch, A. Pelissetto, P. Rossi, and E. Vicari, *Critical Behavior of the Three-Dimensional XY Universality Class*, Phys. Rev. B **63**, 214503 (2001).
[31] W. Xu, Y. Sun, J.-P. Lv, and Y. Deng, *High-Precision Monte Carlo Study of Several Models in the Three-Dimensional U(1) Universality Class*, Phys. Rev. B **100**, 064525 (2019).
[32] M. Aizenman, R.L. Greenblatt, and J.L. Lebowitz, *Proof of Rounding by Quenched Disorder of First Order Transitions in Low-Dimensional Quantum Systems*, J. Math. Phys., **53**, 023301 (2012).
[33] B. M. McCoy and T. T. Wu, *Theory of a Two-Dimensional Ising Model with Random Impurities. I. Thermodynamics*, Phys. Rev. **176**, 631 (1968).
[34] U. Wolff, *Collective Monte Carlo Updating for Spin Systems*, Phys. Rev. Lett. **62**, 361 (1989).
[35] R. H. Swendsen and J.-S. Wang, *Nonuniversal Critical Dynamics in Monte Carlo Simulations*, Phys. Rev. Lett. **58**, 86 (1987).
[36] R. B. Griffiths, *Nonanalytic Behavior Above the Critical Point in a Random Ising Ferromagnet*, Phys. Rev. Lett. **23**, 17 (1969).
[37] M. Guo, R.N. Bhatt, and D. A. Huse, *Quantum Griffiths Singularities in the Transverse-Field Ising Spin Glass*, Phys. Rev. B **54**, 3336 (1996).
[38] H. Rieger and A.P. Young, *Griffiths Singularities in the Disordered Phase of a Quantum Ising Spin Glass*, Phys. Rev. B **54**, 3328 (1996).
[39] H. Rieger and N. Kawashima, *Application of a Continous Time Cluster Algorithm to the Two-Dimensional Random Quantum Ising Ferromagnet* Eur. Phys. J. B **9**, 233 (1999)